A Dual Wave Infrared Imaging Polarimeter

J. Larry Pezzaniti*[a], Brett Hokr[b], Jenny F. Niles[b], Rich Edmondson[a], Michael Roche[a], Lisa Blackwell[a]
[a] Polaris Sensor Technologies, 200 Westside Sq., Huntsville, AL, USA 35801;
[b] US Army Space and Missile Defense Command, Huntsville, AL

ABSTRACT

Detection of targets using thermal camera during thermal cross-over periods. Under these conditions, the target takes on the apparent temperature of objects in the foreground or background and becomes undetectable. It is commonly said that the thermal imagery is "washed-out". When the thermal contrast of an object against its background is zero, many times a polarization contrast of the same object is non-zero. In this paper, we introduce a camera that measures thermal and polarization images in both the mid-wave infrared (MWIR) and long-wave infrared (LWIR). We also show example images and derive a simple equation that explains the conditions under which a polarization signature of an object can be expected.

Keywords: polarimetry, infrared, Stokes image, MWIR, LWIR, polarization, polarimeter

1. INTRODUCTION

In this paper we describe a mid-wave infrared (MWIR), long-wave infrared (LWIR) dual wave imager with on demand polarization sensing capability (DIPOD). The imager has a very narrow FOV and is designed for imaging small airborne objects at stand-off distances between 2 and 7km. Example data from the sensor will be provided and a theoretical underpinning for the origin of the polarization signature will be presented.

There are many scenarios in which standard thermal imaging in the mid-wave infrared (MWIR) and the long-wave infrared (LWIR) is not optimal. For example, at certain times of the day, the apparent temperature of the object of interest can match the apparent temperature of the surrounding background, and the object can be very difficult to see in the thermal image. These events are often referred to as thermal cross-over periods and typically occur in the morning (during thermal loading) and in the evening near sunset. **Figure 1** compares a LWIR thermal image and an image based on polarization of a tank in an open field during a thermal cross-over event.[i] The top image is the thermal image. The spatial frequencies in the image of the tank are very similar to the dirt, grass and sage brush surrounding the tank. Furthermore, the tank is approximately the same apparent temperature as the surrounding background. As a result, the tank blends into the background and becomes virtually invisible. In the polarization image however, the tank is clearly visible. It is still

Figure 1 Comparison of a thermal LWIR image to LWIR polarimetric image during a thermal cross-over event.

visible in the polarization image because polarization is sensitive to the tanks surface roughness and its surfaces aspect geometries, which are different than the surrounding background.[ii,iii] During night operations, low contrast conditions are typically the rule and not the exception. Polarization sensing is especially needed for night operations because without the sun, objects tend to take on the temperature of their surroundings

Another issue that hinders thermal cameras is background clutter. The target of interest can often have the similar apparent temperature, size and even shape of surrounding background. The image pair in the top of **Figure 2** shows a thermal image (leftmost image) and a polarization image (rightmost image).[i] In the thermal image, the target of interest is the same size shape and apparent temperature of the surrounding juniper trees and sage brush. It is very difficult to find the vehicle in the thermal mode. However, in the polarimetric mode, the vehicle is clearly visible. Again, this is because the polarization image is based on surface geometries and roughness, different phenomena than that which produces the thermal image.

In the lower image pair in Figure 2, the targets are intentionally obscured with tarps designed to blend into thermal background.[i] Again, because polarization is based on different physics, the tarps are visible even when invisible in the thermal image.

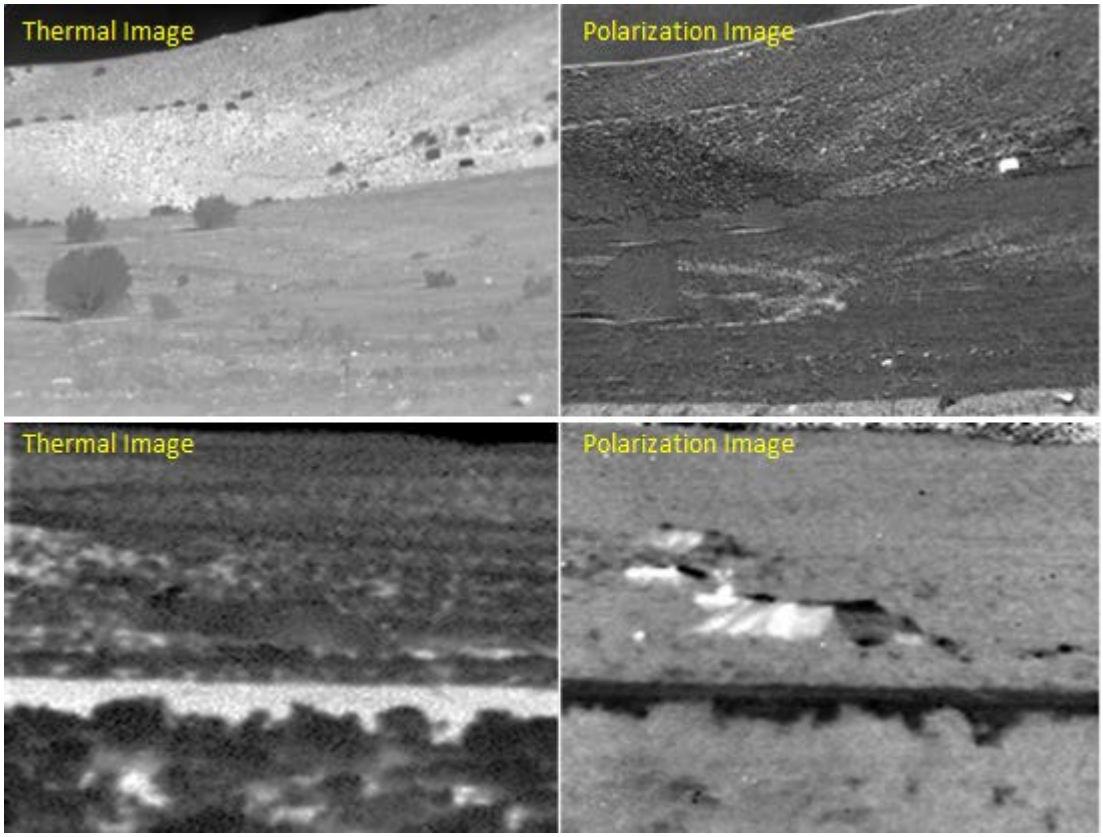

Figure 2 Thermal (left column) vs Polarimetric (right column) in clutter and low contrast conditions.

2. DIPOD SENSOR

DIPOD is a Dual wave (MWIR/LWIR) Imaging Polarimeter with On Demand polarization sensing (DIPOD). DIPOD uses a MWIR/LWIR FPA developed by Night Vision Labs under the

under the US Army Vital Infrared Sensor Technology Acceleration Program (VISTA) program. The specifications for DIPOD are given in **Table 1**. The "on-demand" polarization capability allows the polarization optics (which have ~55% light attenuation) to be removed for thermal only mode operation, thereby enabling optimal performance under all conditions.

Figure 3 shows an image of DIPOD which has a linear wire grid polarizer that rotates synchronously with the FPA image capture. Images are captured every 45 degree orientation of the linear polarizer at horizontal, 45°, vertical and 135° orientations.

The images captured at these orientations of polarization are used to determine the Stokes images of the scene. The Stokes images are defined as

$$\begin{aligned} s_0 &= I_H + I_V \\ s_1 &= I_H - I_V \\ s_2 &= I_{45} - I_{135} \end{aligned} \quad (1)$$

where $I_H, I_V, I_{45}, I_{135}$ are images linearly polarized in the Horizontal, Vertical, 45° and 135° orientations. Note that the s_0 image is simply the standard thermal image. The s_1 and s_2 images are often useful data products in and of themselves to view. However, additional data products derived from these three are often selected. For example, the degree of linear polarization (DOLP) image is often used for target detection, background suppression, and image contrast enhancement. DOLP is given by,

$$DOLP = \sqrt{s_1^2 + s_2^2}. \quad (2)$$

The linear polarizer is inserted between the objective lens and cold shield of the FPA as close to the FPA as possible to eliminate narcissus. The linear polarizer is able to flip into and out of the beam as desired to operate in polarization sensing mode or thermal mode. When the linear polarizer is flipped out of the optical train, an AR coated window with identical thickness and material is flipped into the beam to maintain focus. Figure 4 shows a CAD model of the linear polarizer and window assembly. The linear polarizer and window can be swapped in approximately 0.5 sec. A locking assembly is employed after a movement of the polarizer.

Table 1 Specifications for DIPOD

Parameter	Value
Waveband	3.7-5.1μm & 7.5-10.4μm
Pixel Format	1280 x 720
Pixel Pitch	12.0 μm
Frame Rate	60 Hz
f/#	3
Objective Focal Lengths	200mm, 600mm
FOV (200mm)	4.4° x 2.5°
FOV (600mm)	1.5° x 0.83°
Sensing modes	Thermal + Polarimeter
Polarimetric products	S_1, S_2, DOLP
Integrated Tracking Mount	PVPAEO NightHawk gimbal

Figure 3 DIPOD sensor with 600mm EFL objective lens.

It is important to note that since measurements of polarization are captured sequentially in time that when there is motion in the scene, registration between subsequent images is sometimes

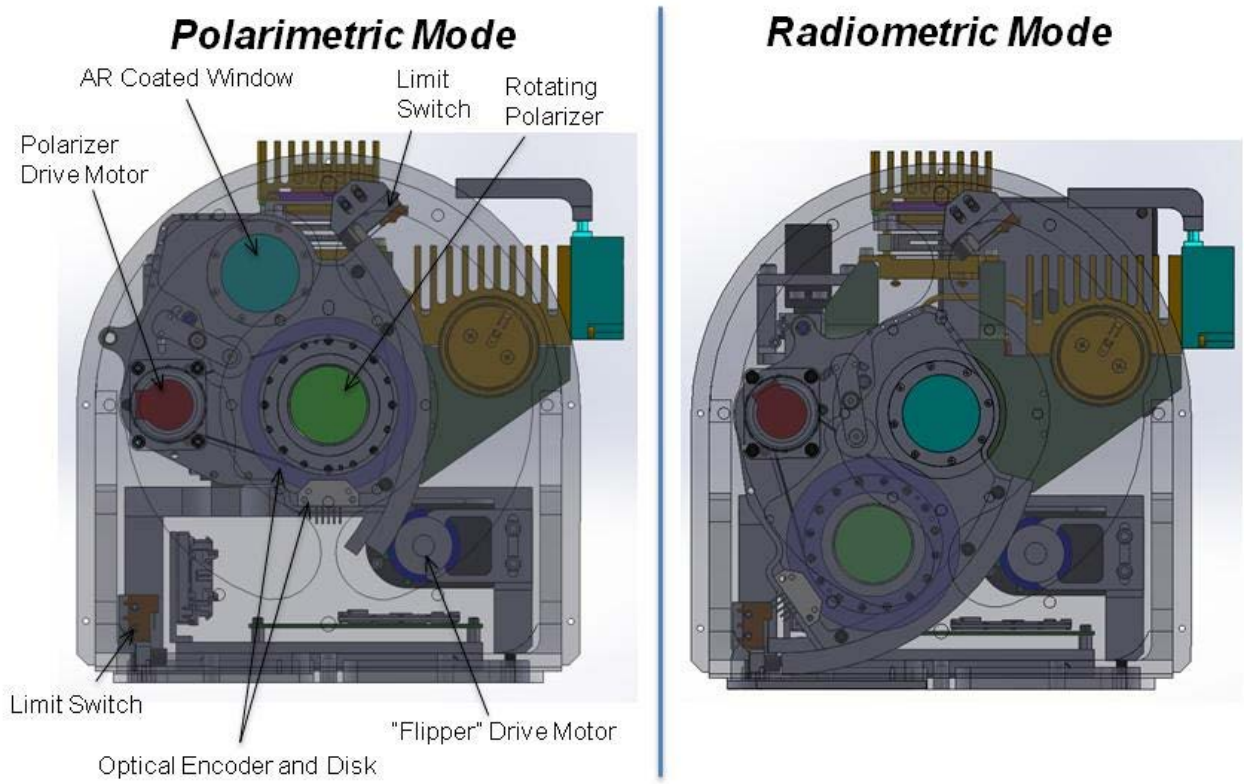

Figure 4 DIPOD with linear polarizer that can be flipped into and out of optical train.

impractical. In this event, it is the flickering of the target in the scene based on its polarization state that is used to identify objects with polarization.

The DIPOD sensor is designed to work with two different objective sets, a 200mm and a 600mm reflective/refractive objective lenses. The two different focal length configurations share the same refractive lens set. The sensor system was designed such that the 200mm and 600mm reflective optics can be swapped in the field. The 600mm relay set weighs approximately 15-kg and protrudes approximately 38-cm from the face of the sensor body. The mounting bracket that holds the objectives was designed to be highly rigid, yet lightweight. The mounting bracket was machined from a single piece of 6061-T6 Aluminum. A basic finite element analysis (FEA) was run and to determine the max deflection due to the moment arm created by the 600mm objective.

3. POLARIZATION SIGNATURE

In the visible portion of the spectrum, the polarization signature of a specular surface depends on the Fresnel reflection coefficients that in turn depend on refractive index of the surface at a particular wavelength and angle of incidence. In the IR portion of the spectrum the emission polarization of the surface must also be considered. Here we model the reflection and emission polarization of a spectral surface. The polarization signature is related to the complex refractive index, the

background apparent temperature and the sample temperature. The modeled predictions are then compared to measurements with a LWIR imaging polarimeter.

The Stokes vectors are typically used to describe the polarization state of light. If we consider the geometry in **Figure 5**, the s and p polarization states are related to the S_1 Stokes vector by

$$S_1 = \frac{L_s(\theta,\lambda,T_0,T_B) - L_p(\theta,\lambda,T_0,T_B)}{L_s(\theta,\lambda,T_0,T_B) + L_p(\theta,\lambda,T_0,T_B)} \tag{3}$$

where $L_s(\theta,\lambda)$ is the s-state radiance [Watts/cm^2-sr-μm] emanating from the water surface and $L_p(\theta,\lambda)$ is the p-state polarization state radiance emanating from the water surface, and θ is the ray angle associated with a field point emanating at an angle normal to the back-body source, and λ is the wavelength of the radiation. The s- and p- state spectral radiance L_s and L_p are given by

$$\mathrm{L_S}(\theta,\lambda,T_0,T_B) = P(T_0,\lambda)\,\varepsilon_S(\theta,\lambda) + P(T_B,\lambda)\,\varepsilon_B(\lambda)\,R_S(\theta,\lambda) \tag{4}$$

$$\mathrm{L_p}(\theta,\lambda,T_0,T_B) = P(T_0,\lambda)\,\varepsilon_p(\theta,\lambda) + P(T_B,\lambda)\,\varepsilon_B(\lambda)\,R_p(\theta,\lambda) \tag{5}$$

where,

$$P(T,\lambda) = \frac{2\pi hc}{\lambda^5}\cdot\frac{1}{exp^{\left(hc/\lambda kT\right)}-1} \tag{6}$$

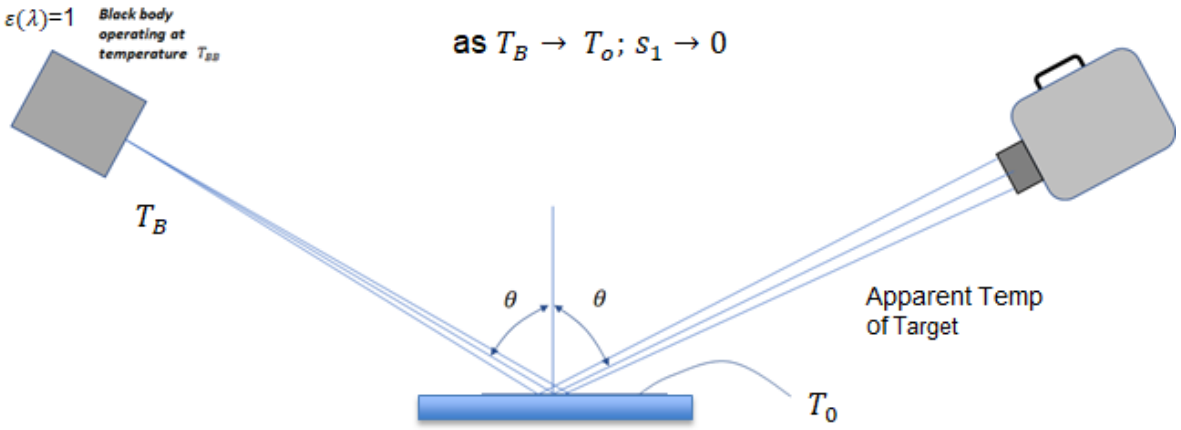

Figure 5 Setup to measure S1 signature of water, where background temp and water temp are controlled.

$\varepsilon_S(\theta,\lambda)$ and $\varepsilon_p(\theta,\lambda)$ are the s- and p- polarized emissivities of the surface, $R_S(\theta,\lambda)$ and $R_p(\theta,\lambda)$ are the s- and p- polarized reflectances of the surface and $\varepsilon_B(\lambda)$ is the emissivity of the black body emitter at normal emission angle.

Once a body reaches thermal equilibrium with its surroundings, the first law of thermodynamics requires that

$$\Phi_{incident} = \Phi_{absorbed} + \Phi_{transmitted} + \Phi_{reflected} \tag{7}$$

where $\Phi_{incident}$ is the incident flux on the surface. Dividing both sides of Eqn. 4 by $\Phi_{incident}$ yields

$$1 = \alpha + \tau + R \tag{8}$$

where α is the absorptance, τ is the transmittance, and R is the reflectance.

To validate the model of polarization we measured the S1 polarization of water as a function of angle of incidence as depicted in **Figure 5.** **Figure 6** shows the absorption coefficient and penetration depth of water in the infrared. In the 7.5 to 10.4 mm region, the penetration depth of water is approximately 20 μm.

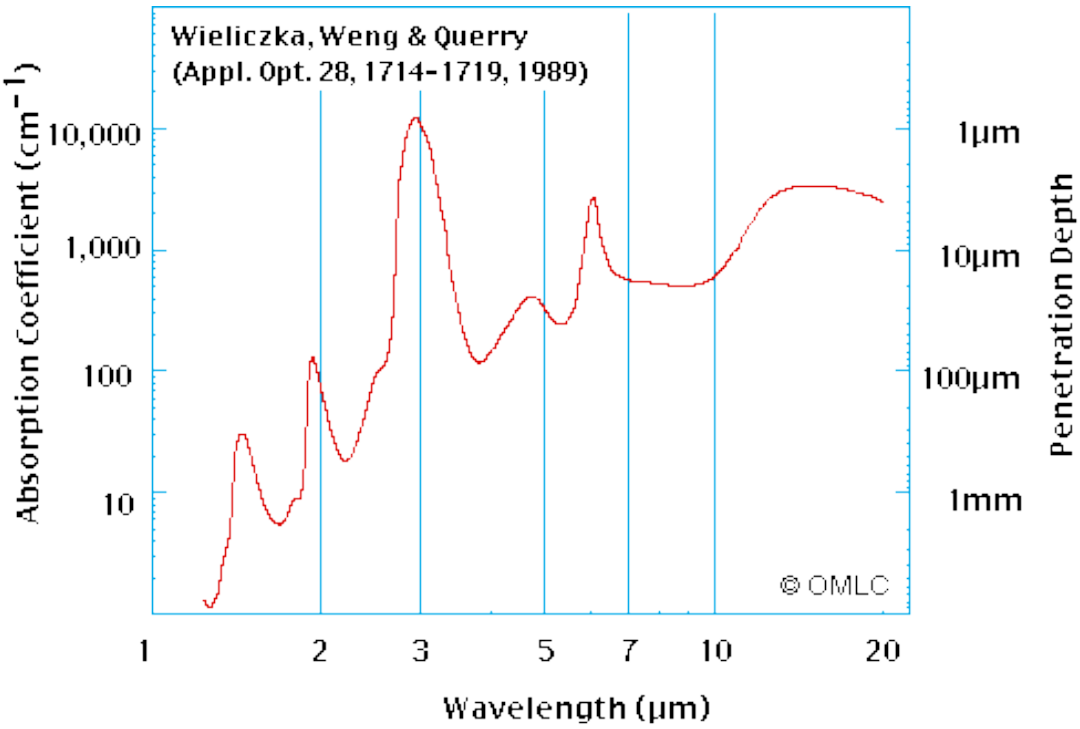

Figure 6 absorption coefficient and penetration depth of water.

For a highly absorptive medium such as water in the infrared, $\tau = 0$ and Eqn. 8 becomes

$$\alpha + R = 1 \tag{9}$$

Now, Kirchhoff's law states that the absorbance of a surface is identical to the emissivity of that surface. That is the emissivity ϵ, is given by

$$\varepsilon = \alpha \tag{10}$$

and,

$$\alpha = 2\pi k/\lambda_o \tag{11}$$

Kirchhoff's law also holds spectrally and can vary with the direction of measurement. Thus, we have,

$$\varepsilon(\theta, \lambda) + R(\theta, \lambda) = 1 \tag{12}$$

If a light field is s- or p- state polarized, Eqn. 9 will also hold. Therefore, we have,

$$\varepsilon_s(\theta,\lambda) + R_s(\theta,\lambda) = 1 \quad (13)$$

and,

$$\varepsilon_p(\theta,\lambda) + R_p(\theta,\lambda) = 1 \quad (14)$$

Therefore, we have,

$$\varepsilon(\theta,\lambda) = \frac{1}{2}\left(\varepsilon_s(\theta,\lambda) + \varepsilon_p(\theta,\lambda)\right) \quad (15)$$

$$R(\theta,\lambda) = \frac{1}{2}\left(R_s(\theta,\lambda) + R_p(\theta,\lambda)\right) \quad (16)$$

Given Equations (10) and (11), we can rewrite Equations (2) and (3) as

$$L_S(\theta,\lambda,T_0,T_B) = P(T_0,\lambda)(1 - R_S(\theta,\lambda)) + P(T_B,\lambda)\,\varepsilon_B(\lambda)\,R_S(\theta,\lambda) \quad (17)$$

and,

$$L_p(\theta,\lambda,T_0,T_B) = P(T_0,\lambda)\,(1 - R_p(\theta,\lambda)) + P(T_B,\lambda)\,\varepsilon_B(\lambda)\,R_p(\theta,\lambda) \quad (18)$$

$$s_1(\theta,\lambda,T_0,T_b) = \frac{\left(R_s(\theta,\lambda) - R_p(\theta,\lambda)\right)\cdot\left(P(T_B,\lambda)\cdot\varepsilon(\lambda) - P(T_0,\lambda)\right)}{2P(T_0,\lambda) + \left(R_s(\theta,\lambda) + R_p(\theta,\lambda)\right)\cdot\left(P(T_B,\lambda)\cdot\varepsilon(\lambda) - P(T_0,\lambda)\right)} \quad (19)$$

Figure 7 is a family of s_1 curves with a background black body temperature of 35C, and a water sample temperature of 19C, between wavelengths of 7.4μm and 10.4μm and as a function of ray angle of incidence θ. The complex refractive indices for water used to compute Rs and Rp were taken from Palik.[iv] **Figure 8** shows a measurement of the same water surface at the same temperature with a background black body temperature 15C. Note that the shape of the curve remains unchanged, but the sign has changed. This is explained with Equation 19. When the temperature of the target surface and the background changes, the term ($R_s(\theta,\lambda)$-$Rp(\theta,\lambda)$) does not change because it is weakly dependent on temerpature. The term ($P(T_B,\lambda)$-$P(T_0,\lambda)$) changes in magnitude but does not change the angle of incidence dependence. When $T_B > T_0$, the curve is positive sign. When $T_B < T_0$, the curve is negative sign.

Figure 9 shows the same curves for a flat surface of a Phantom IV octocopter that is at 24C. The plot on the left shows S_1/S_0 at three different angles of incidence 65, 75 and 85o as a function of background temperature. Note that for background temperatures below 24C, the S_1/S_0 value is negative for reasons given above. For background temperatures above 24C, the S_1/S_0 signature is positive. At background temperature at exactly 24C, the S_1/S_0 signature is always zero.

This behavior is common to any surface that is optically smooth in infrared. These surfaces include manmade objects such as metals, plastics, glass, painted surfaces, processed wood. The polarization contrast depends on the difference between the target temperature and the reflected background, whereas thermal contrast depends on the difference between the target temperature and the surrounding background.

Therefore, the polarization sensing mode requires different contrast conditions between the target and background than thermal imaging. When an object's apparent temperature blends into the surrounding background making it impossible to detect in thermal mode, often times the reflected background is still different enough to detect the object in polarization mode.

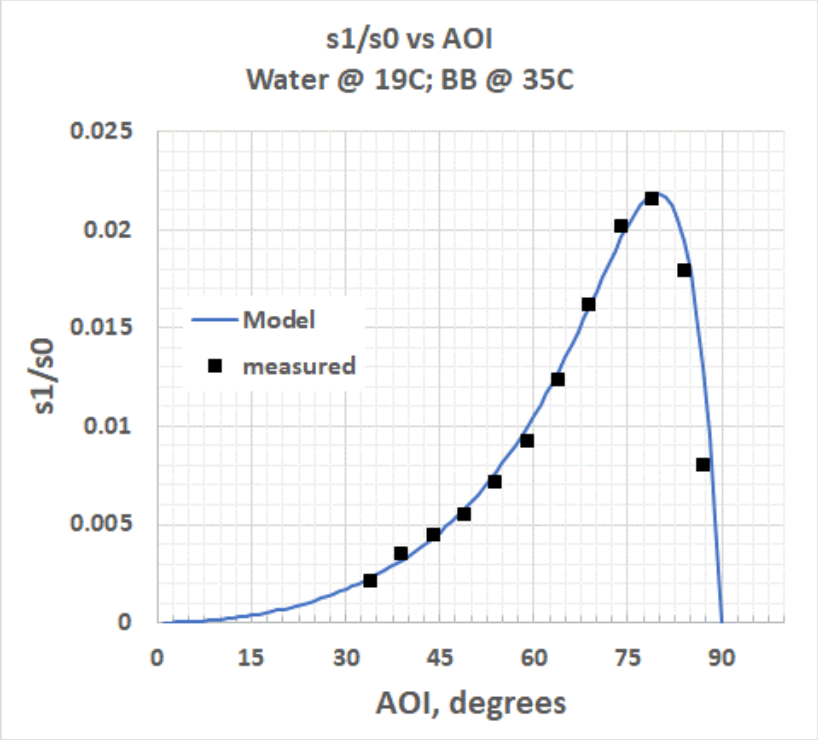

Figure 7 S_1/S_0 of water surface at temperature 19C reflecting background at 35C.

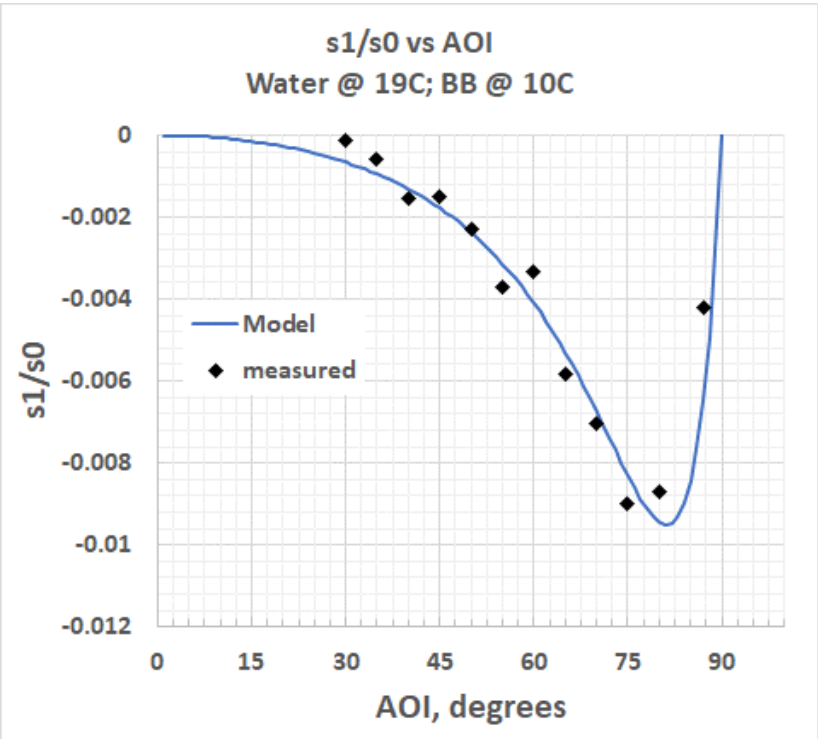

Figure 8 S_1/S_0 of water surface at temperature 19C reflecting background at 10C.

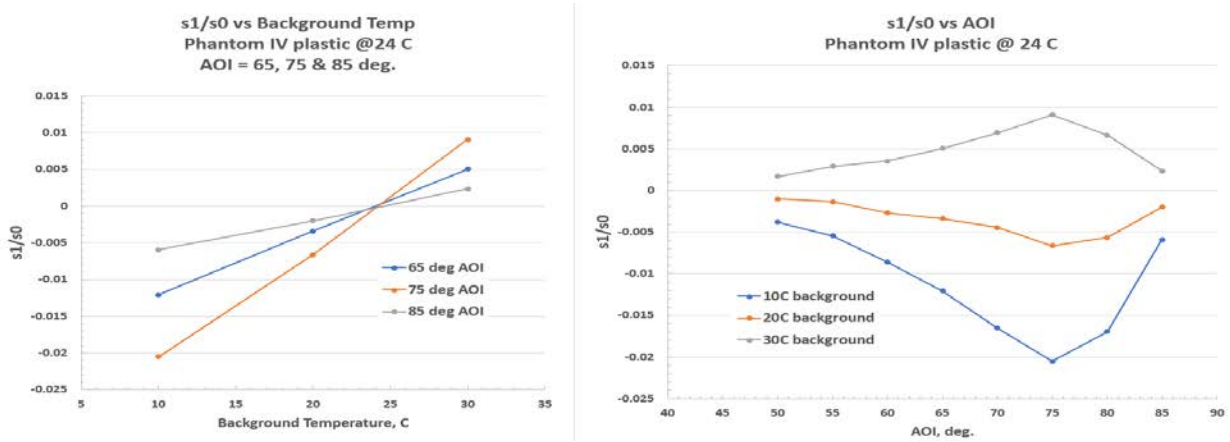

Figure 9 Polarization signature of a Phantom IV octocopter vs background temperature.

4. EXAMPLE IMAGES FROM DIPOD

Figures 10 and **11** show example data from DIPOD in the MWIR and LWIR portion of the spectrum. The aspect angle of the octocopter was varied to understand how the signature changes when viewing the craft at different aspect angles. The angle to the left of each row indicates the look-up angle of the sensor while the craft is oriented horizontally.

In both the MWIR and LWIR, the underside of the craft is un-polarized ($S_1/S_0=0$). The reason for these zero signatures is that the ground is at approximately the same apparent temperature as the underside of the octocopter. According to Eq. 19, the signature should equal zero. The top of the octocopter however reflects cold sky, and has a non-zero S_1/S_0 signature. The S1 and S2 signatures are variable on the top surface of the craft because the surface normal varies with its shape.

The DOLP images clearly show that clouds in the MWIR portion of the spectrum have non-zero DOLP, whereas the DOLP is zero in the LWIR. Modeling is ongoing to understand this phenomenon, but it is currently postulated from MIE scattering theory that the size distribution of the cloud particles are such that the polarization is coming from single scatter from the outer surface of the cloud.

5. CONCLUSIONS

A dual wave imaging polarimeter that operates in the MWIR and LWIR portions of the spectrum was developed. Validation of the sensor and modeling was validated through measurements of water in the laboratory where the water temperature and background temperature were controlled. The analysis and measurement shows that the polarization signature of an optically smooth surface depends on the complex refractive indices of the surface, its temperature and the apparent temperature of the background reflecting off of the surface. DIPOD was also used to measure the polarization signatures of a Phantom IV quadcopter and the results were interpreted based on the modeling provided.

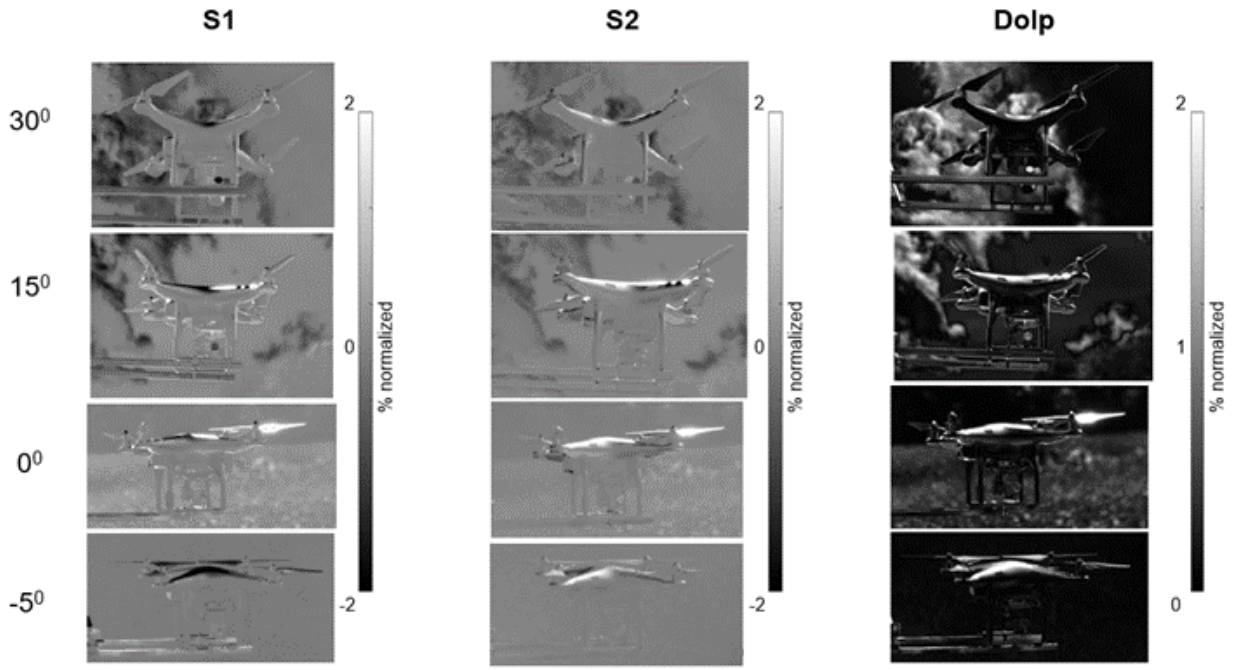

Figure 10 MWIR Stokes images of a Phantom IV octocopter at different viewing angles. The top row of images corresponds to looking up at the octocopter that is flying horizontally at a 30º degree angle. The aspect angles of 15º, 0º and -5º correspond to look angles slightly up, horizontal and down looking respectively.

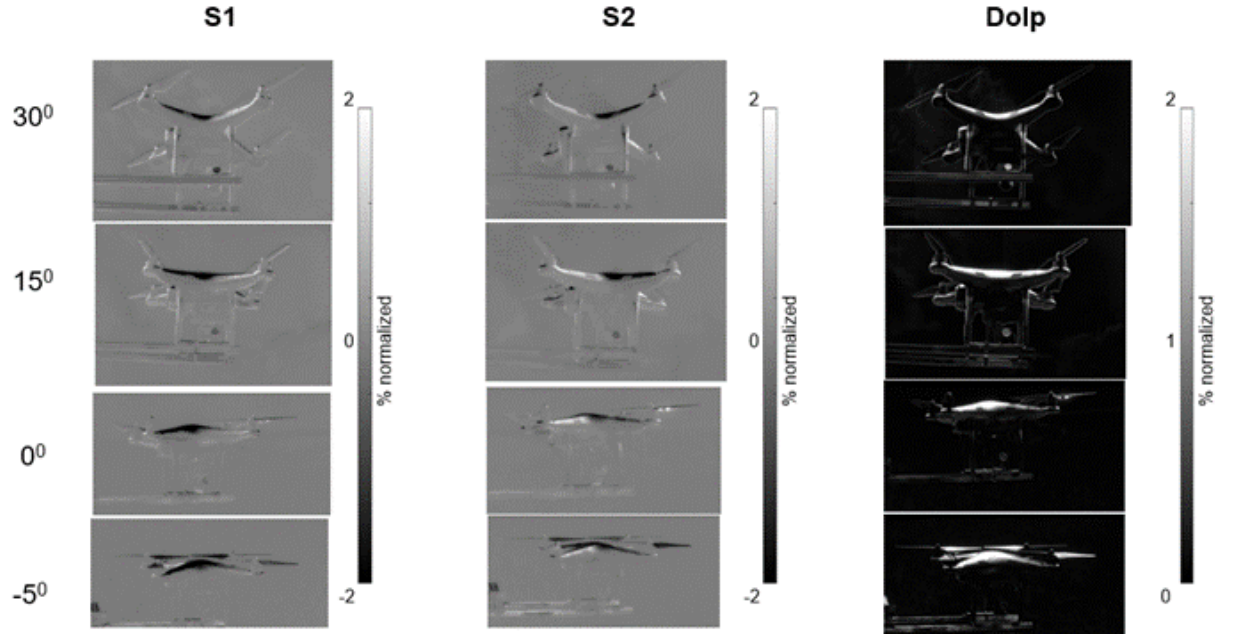

Figure 11 LWIR Stokes images of a Phantom IV octocopter at different viewing angles. The top row of images corresponds to looking up at the octocopter that is flying horizontally at a 30º degree angle. The aspect angles of 15º, 0º and -5º correspond to look angles slightly up, horizontal and down looking respectively.

References

[i] J. L. Pezzaniti, D. Chenault, K.Gurton, M. Felton, "IR Polarimetric signatures," SPIE DSS, May 2014, Active and Passive Signatures V, article 9082-3.
[ii] M. Felton, K. P. Gurton, J. L. Pezzaniti, D. B. Chenault, and L. E. Roth, "Measured comparison of the crossover periods for mid- and long-wave IR (MWIR and LWIR) polarimetric and conventional thermal imagery, Optics Express, Vol. 18. Issue 15, pp. 15704-15713 (2010).
[iii] Comparison of the inversion periods for MidIR and LWIR polarimetric and conventional thermal imagery, M. Felton, K. P. Gurton, J. L. Pezzaniti, D. B. Chenault, L.E. Roth, SPIE 7672, (2010).
[iv] E. D. Palik, "Handbook of Optical Constants of Solids," Academic Press, 1998, pp. 1067-1077.